Scientific Research Publishing

Detection, 2018, 6, 1-16
http://www.scirp.org/journal/detection
ISSN Online: 2331-2084
ISSN Print: 2331-2076

Study on the Theoretical Limitation of the Mid-Infrared PbSe N$^+$-P Junction Detectors at High Operating Temperature

Xinghua Shi[1*], Quang Phan[1], Binbin Weng[1], Lance L. McDowell[1], Jijun Qiu[1,2], Zhihua Cai[1,2], Zhisheng Shi[1*]

[1]The School of Electrical and Computer Engineering, University of Oklahoma, Norman, USA
[2]Nanolight, Inc., Norman, USA
Email: *xinghua.shi@ou.edu; shi@ou.edu

How to cite this paper: Shi, X.H., Phan, Q., Weng, B.B., McDowell, L.L., Qiu, J.J., Cai, Z.H. and Shi, Z.S. (2018) Study on the Theoretical Limitation of the Mid-Infrared PbSe N$^+$-P Junction Detectors at High Operating Temperature. *Detection*, **6**, 1-16.
https://doi.org/10.4236/detection.2018.61001

Received: January 2, 2018
Accepted: January 28, 2018
Published: January 31, 2018

Abstract

This paper provides a theoretical study and calculation of the specific detectivity-D^* limit of photovoltaic (PV) mid-wave infrared (MWIR) PbSe n^+-p junction detectors operating at both room temperature and TE-cooled temperature. For a typical PbSe p-type doping concentration of 2×10^{17} cm^{-3} and with high quantum efficiency, the D^* limits of a photovoltaic PbSe n^+-p junction detector are shown to be 2.8×10^{10} HZ$^{1/2}$/W and 3.7×10^{10} HZ$^{1/2}$/W at 300 K and 240 K, with cut-off wavelength of 4.5 μm and 5.0 μm, respectively. It is almost one magnitude higher than the current practical MWIR PV detector. Above 244 K, the detector is Johnson noise limited, and below 191 K the detector reaches background limited infrared photodetector (BLIP) D^*. With optimization of carrier concentration, D^* and BLIP temperature could be further increased.

Keywords

PbSe, Lifetime, R_0A, Detectivity

1. Introduction

The MWIR light detection has widespread applications in the fields of health monitoring, environmental protection, defense and national security, as well as space exploration and other fields. Existing technologies with high sensitivity are mainly based on semiconductor photo-detectors. In the past half-century, many semiconductor material systems have been intensively studied, and significant progress has been made [1] [2]. Currently, the leading photodetector approaches

are mainly based on HgCdTe (MCT) [3] [4] III-V type-II superlattices, and InSb-based material systems. Among them, MCT is the premier material of interest for MWIR Focal Plane Arrays (FPA) applications. The challenges have been reducing the cost, size, weight, and power requirements, while improving the detection range and resolution. So far, these MWIR FPAs still require cryogenic cooling to achieve high detectivity, which is bulky and expensive. It is known that the major fundamental hurdle of the MWIR photodetectors at high operation temperature is the high Auger recombination rate. Among these detectors, the MCT technology has demonstrated its state-of-the-art performance, which is closely approaching the Auger theoretical limit.

It is well known that Auger coefficient in IV-VI semiconductors [5] [6] [7] is about an order of magnitude lower than those in Sb-based type-II QWs, [8] [9] [10] which are in turn significantly suppressed relative to other III-V and II-VI semiconductors such as MCT [11] [12] for the same waveleng. Such low Auger recombination should result in superior device performance such as high detectivity for detectors at a high operating temperature. High specific detectivity (D^*) of PbSe MWIR photoconductive (PC) detector at room temperature was reported, 2.8×10^{10} cm·Hz$^{1/2}$/W and 4.2×10^{10} cm·Hz$^{1/2}$/W at ~3.8 μm, with and without antireflective coating [13] [14] [15]. Northrop Grumman has demonstrated monolithic integrated PbSe PC detector FPA with Si read-out circuitry (ROIC) with thermoelectric (TE) cooling [16]. These exciting results have stimulated renewed interests in using Pb-salt cameras for TE-cooled or uncooled applications [17].

It is worth nothing that photovoltaic (PV) detectors offer advantages over their PC detector counterparts, such as low power consumption, high pixel density, and small pixel size. In addition, a PV detector FPA operating at low bias with no or low flicker noise eases the design of ROIC which further reduces cost. Although the D^* of the IV-VI Pb-salt semiconductor junction at a low temperature has been investigated via experimental and theoretical research, the performance limit of PbSe at high temperature has not been well investigated. In this paper, we investigate the performance limit of a PbSe n^+-p junction detector operating at room temperature and TE-cooled temperature.

2. The Specific Detectivity D^*

Specific detectivity, or D^*, for a photodetector is an important figure of merit and is determined by [18]:

$$D^* = \frac{\sqrt{A\Delta f}}{NEP} \tag{1}$$

where A is the active area of the detector and NEP is the noise equivalent power (the power needed to generate the signal current which is equal to the noise current)

$$NEP = \frac{\Phi_e}{i_{sig}/i_n} \tag{2}$$

Here Φ_e [19] is the radiant power incident on a detector.

In a junction device, the fluctuation of diffusion rates in the neutral region and the generation-recombination (g-r) fluctuation in both depletion region and quasi-neutral region are indistinguishable. All of them give rise to the shot noise which has the form of [20]

$$i_n^2 = 2q\left(I_D + 2I_S\right)\Delta f \tag{3}$$

where I_D is the diode current, I_S is the dark reverse-bias saturation current of the device and Δf is the electrical bandwidth.

$$I_D = I_S \times \left(\mathrm{e}^{\frac{qV}{\beta kT}} - 1 \right) \tag{4}$$

β is the ideality factor which determines how the actual diode deviates from the ideal diode. In most of our later calculations, we assume the ideal diode case where $\beta = 1$.

For the diode under the illumination of photon density flux Φ_b, which generates the photon current $I_{ph} = q\eta A\Phi_b$, the total noise contribution is:

$$I_n^2 = 2q\left(q\eta A\Phi_b + \frac{kT}{qR_0}\mathrm{e}^{\frac{qV}{kT}} + \frac{kT}{qR_0} \right)\Delta f \tag{5}$$

where R_0 is the zero-voltage resistance which is defined by

$$R_0 = \left(\frac{\partial I_D}{\partial V} \right)_{V=0}^{-1} = \frac{kT}{qI_S} \tag{6}$$

Under the zero-voltage case, the expression of shot noise in (3) has the same form as the Johnson-noise associated with the R_0 of the junction, thus it is often called Johnson noise.

Substituting (1) and (2) to (5), the expression for the detectivity of the device is

$$D^* = \frac{q\eta\lambda}{hc}\left[\frac{4kT}{R_0 A} + 2q^2\eta\Phi_b \right]^{-1/2} \tag{7}$$

In Equation (7), η is the quantum efficiency, λ is the wavelength of the incident radiation, q is the charge of the carrier, h is Planck's constant, c is the speed of light, k is Boltzmann's constant, R_0 is the diode incremental resistance at 0 V, A is the detector sensitive area, T is the temperature of the detector in Kelvin, and Φ_b is the photon flux incident on the detector from its surroundings. It is clear that both R_0A and η are key factors on the specific detectivity D^*. Therefore, the resistance-area (R_0A) product at zero bias needs to be calculated to determine D^* based on Equation (6).

3. R_0A Analysis and Discussions

The total dark current density flowing through the junction can be found with the following equation:

$$J_s = \frac{I_s}{A} = J_{DF} + J_{GR} + J_T + J_L \tag{8}$$

In Equation (7), J_{DF} is the diffusion current density, J_{GR} is generation-recombination current density that is often dominated in the depletion layer, J_T is tunneling current density and J_L is leakage current density. J_L may be due to bulk as well as surface defects of the material. When suitable diode technology and construction are used, the contribution of the J_L component is negligible.

The maximum R_0A is obtained from the one-sided abrupt junction [21], giving the limitation on the specific detectivity D^*. The minority carriers on the lightly doped side of the n^+-p junction will dominant the diffusion current. The R_0A product determined by the diffusion current in the case of radiative recombination and Auger recombination is

$$\left(R_0A\right)_{DF} = \frac{\left(kT\right)^{1/2}}{q^{3/2}n_i^2} N_A \left(\frac{\tau_e}{\mu}\right)^{1/2} \tag{9}$$

where n_i is the intrinsic carrier concentration, $N_A(N_D)$ is the concentration of donors (acceptors), $\tau_h(\tau_e)$ is the minority carrier lifetime of holes (electrons) and $\mu_h(\mu_e)$ is the minority carrier mobility.

The resistance-area product (R_0A) of PbSe photo-voltaic detectors under conditions of zero bias is calculated for one-side abrupt junction. Highly doped n-side homojunction (n^+-p) is discussed in this paper. At room temperature, the effective R_0A product on the PbSe n^+-p junction can be expressed by:

$$\begin{aligned}\left(R_0A\right)^{-1} &= \left(R_0A\right)_{DF}^{-1} + \left(R_0A\right)_T^{-1} + \left(R_0A\right)_{SRH}^{-1} \\ &= \left(R_0A\right)_{RA}^{-1} + \left(R_0A\right)_{Auger}^{-1} + \left(R_0A\right)_T^{-1} + \left(R_0A\right)_{SRH}^{-1}\end{aligned} \tag{10}$$

where $\left(R_0A\right)_{RA}$ is the R_0A product due to radiative recombination, $\left(R_0A\right)_{Auger}$ is the R_0A product due to Auger recombination, and $\left(R_0A\right)_{SRH}$ is the R_0A product due to Shockley-Read-Hall recombination. Different R_0A products due to each recombination mechanism will be discussed in the following section.

3.1. Radiative Recombination Contribution

The R_0A product determined by the diffusion current in the case where radiative recombination has the relationship on the lifetime τ_r^{-1}. The radiative lifetime τ_r^{-1} for PbSe follows as [22]:

$$G_R = 10^{-15} n_r \left(kT\right)^{-\frac{3}{2}} \left(2 + \frac{1}{K}\right)^{-\frac{3}{2}} \left(\frac{m^*}{m}\right)^{-\frac{5}{2}} \left(K\right)^{-\frac{1}{2}} E_g^2 \,\mathrm{cm}^3/\mathrm{sec}, \quad K = m_l^*/m_t^* \tag{11}$$

$$\tau_r^{-1} = G_R\left(n_0 + p_0\right) \tag{12}$$

$$n_0 + p_0 = 2\left(\frac{N_D^2}{4} + n_i^2\right)^{1/2} \tag{13}$$

The radiative lifetime is inversely proportional to the total concentration of

free carriers under all circumstances. The radiative lifetime decreases when the doping concentration increases.

G_R is the capture probability for radiative recombination. The band gap of a semiconductor E_g is expressed in electron-volts. n_r is the index of refraction, and $m^* = \left[1/3\left(2/m_t + 1/m_l\right)\right]^{-1}$ is the density-of-states electron and hole effective masses. n_i is intrinsic carrier concentration. n_0 and p_0 represent the equilibrium carrier concentrations. According to Equation (14), the $(R_0A)_{RA}$ product can be found after the radiative recombination lifetime is calculated.

$$\left(R_0A\right)_{RA} = \frac{\left(kT\right)^{1/2}}{q^{3/2}n_i^2} N_A \left(\frac{\tau_r}{\mu}\right)^{1/2} \tag{14}$$

Figure 1 describes the radiative life time on the dopant concentrations for the PbSe junction at 300 K. When carrier concentration is between 10^{17} and 10^{18}, the radiative recombination life time of PbSe is between 10^{-7} s and 10^{-8} s at 300 K.

3.2. Auger Recombination Contribution

The R_0A product determined by the diffusion current in the case of Auger recombination has the relationship on the lifetime τ_A^{-1}. The PbSe Auger's recombination coefficient C_A is given by [7]:

$$C_A = \frac{3q^4\left(2\pi\right)^{5/2}\left(k_BT\right)^{1/2}Eg^{-7/2}\hbar^3}{\left(16\pi\varepsilon_0\varepsilon_\infty\right)^2 m_l^{*1/2}m_t^{*3/2}} \times \exp\left[-\frac{Eg}{2k_BT}\left(\frac{m_l^*}{m_t^*}\right)^{-1}\right] \tag{15}$$

where m_l^* and m_t^* are the longitudinal and transverse effective mass, ε_∞ is high frequency dielectric constant, and ε_0 is vacuum permittivity. During the Auger recombination process, the carrier lifetime is defined as:

$$\tau_A = \left[C_A\left(N_A^2 + 2n_i^2\right)\right]^{-1} \tag{16}$$

Figure 2 shows the Auger life time of different dopant concentrations for the PbSe junction at room temperature. When carrier concentration is between 10^{17}

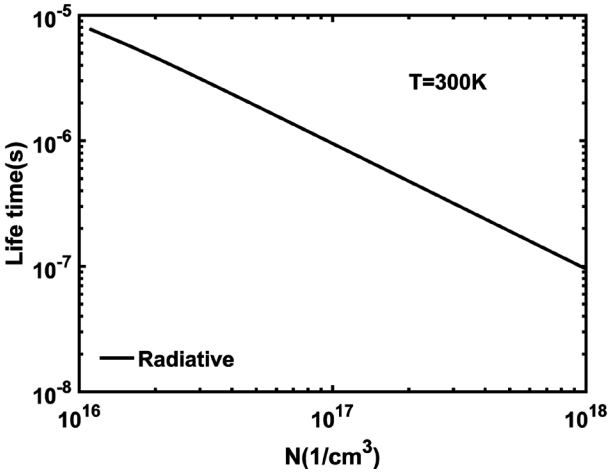

Figure 1. The dependence of the radiative life time on the dopant concentrations for the PbSe junction at 300 K.

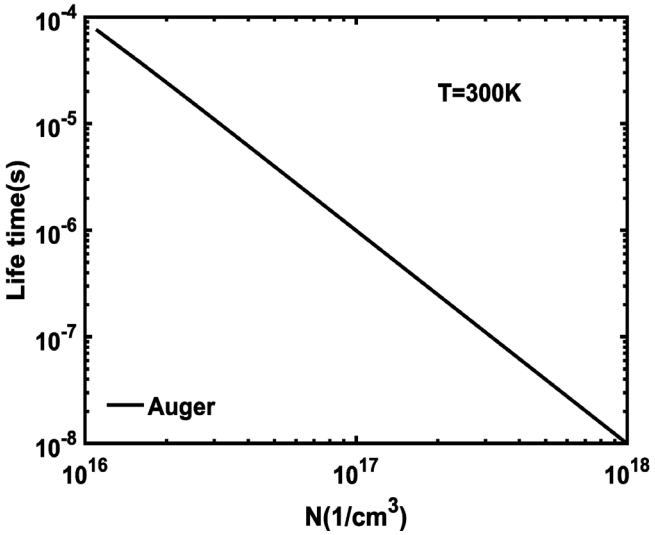

Figure 2. The dependence of the Auger life time on the dopant concentrations for the PbSe junction at 300 K.

and 10^{18}, the Auger recombination life time of PbSe is between 10^{-7} s and 10^{-8} s at 300 K. According to Equation (17), the $(R_0A)_{Auger}$ product can be derived when the Auger recombination lifetime is calculated.

$$\left(R_0A\right)_{Auger} = \frac{\left(kT\right)^{1/2}}{q^{3/2}n_i^2} N_A \left(\frac{\tau_A}{\mu}\right)^{1/2} \tag{17}$$

3.3. Tunneling Current Contribution

The $(R_0A)_T$ determined by tunneling is given by

$$\left(R_0A\right)_T = 4*\pi^3\hbar^2\left(\varepsilon_s\varepsilon_0\right)^{\frac{1}{2}} \exp\left[\frac{\pi\left(m_x\varepsilon_s\varepsilon_0\right)^{\frac{1}{2}} Eg}{2^{\frac{3}{2}} q\hbar N_D^{\frac{1}{2}}}\right] \Bigg/ \left(q^3\sqrt{\frac{2N_A m_y m_z}{m_x}}\right) \tag{18}$$

Tunneling simulation of PbSe depends on the crystal orientation due to the difference in effective masses. The four effective masses to consider are: m_{el} (conduction band, longitudinal), m_{et} (conduction band, transverse), m_{hl} (transverse band, longitudinal) and m_{ht} (transverse band, transverse). m_0 is the electron resting mass [23].

$$m_{el} = \left[11.4\times\frac{0.145}{Eg}+2.9\right]^{-1}\times m_0$$

$$m_{et} = \left[20.7\times\frac{0.145}{Eg}+4.3\right]^{-1}\times m_0$$

$$m_{hl} = \left[11.4\times\frac{0.145}{Eg}+3.3\right]^{-1}\times m_0$$

$$m_{ht} = \left[20.7\times\frac{0.145}{Eg}+8.7\right]^{-1}\times m_0$$

For PbSe [100] directions, the effective mass on different orientations can be determined by the Table 1.

In order to compare Auger, radiative and tunneling recombination, R_0A production on those three recombination mechanisms versus different temperatures is analyzed. In the following calculation $N_A = 2\times10^{17}\,\mathrm{cm}^{-3}$, a typical PbSe hole concentration is used. To satisfy n^+-p junction, N_D is chosen to be $1 \times 10^{18}\ \mathrm{cm}^{-3}$, which is five times higher than N_A. Throughout this paper, we use $N_D \geq 5N_A$ for our n^+-p junction calculation. Looking at Figure 3(a) for the given carrier concentration $N_A = 2\times10^{17}$, at a higher temperature, $(R_0A)_T$ increases significantly for the PbSe [100] junction so that the tunneling $(R_0A)_T$ can be ignored. This is mainly because the energy bang gap of PbSe increases with temperature. When

Table 1. PbSe [100] effective mass in different directions.

m_x	m_y	m_z
m_t	$\frac{3m_lm_t}{2m_l+m_t}$	$\frac{2m_l+m_t}{3}$

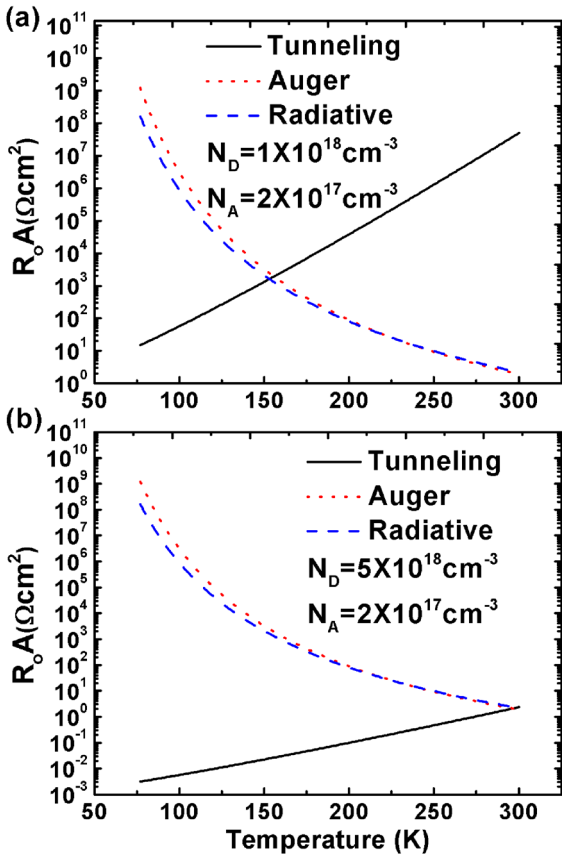

Figure 3. The dependence of the tunneling R_0A product on the dopant concentrations for the PbSe [100] junction at 160 K and 240 K. For Figure 3(a) the n side carrier concentration is $1 \times 10^{18}\ \mathrm{cm}^{-3}$, and in Figure 3(b) n side carrier concentration is $5 \times 10^{18}\ \mathrm{cm}^{-3}$.

the temperature is around 160 K, $(R_0A)_T$ is comparable to the Auger R_0A and radiative R_0A. For even lower temperatures, $(R_0A)_T$ becomes dominant. At temperatures above 180K K $(R_0A)_T$ is at least five times higher than the other mechanisms and thus $(R_0A)_T$ can be neglected relative to the total R_0A product.

To keep the same N_A and increase N_D doping concentrations, **Figure 3(b)** shows that $(R_0A)_T$ cannot be neglected even at room temperature. At about 275 K, $(R_0A)_T$ is five time lower than the other mechanisms and at higher than 275 K tunneling needs to be considered in the total R_0A product. Comparing **Figure 3(a)** and **Figure 3(b)**, it is apparent that carrier concentration has a large influence on R_0A, and therefore, the total device performance.

3.4. SRH Recombination Contribution

The carrier generation-recombination mechanisms in detector devices are distinguished as Auger, radiative, tunneling, and Shockley-Read-Hall's (SRH) generation-recombination mechanisms. Auger, radiative, and tunneling mechanisms are determined by energy band structures. However, SRH's mechanism is determined by the material quality. In Equation (4), the depletion generation and recombination R_0A term is largely dominated by the lifetime associated with SRH centers. However, the value of this lifetime is extremely uncertain as has been noted in previous studies [7] [24]. These studies often assume longer SRH lifetimes in their investigations, typically on the order of 10^{-8}s[25]. Thus, using this assumed SRH lifetime, higher temperature operations produce high values for $(R_0A)_{GR}$ which may be neglected in our case. However, SRH recombination may need to be considered with a shorter SRH lifetime.

3.5. Discussion of the Overall R_0A Limitation

Utilizing the R_0A expressions shown in the above sections, calculations of R_0A for Auger, radiative, and tunneling were described in **Figure 4**. For a fixed operating temperature, R_0A dependence on carrier concentration reveals the contribution of each mechanism, revealing an optimized condition for the maximum R_0A limit. Three temperatures of interest are used. 300 K, 240 K, and 160 K represent temperatures of an uncooled, cut-off wavelength of 5 μm, and that the tunneling effect needs to be considered.

Table 2 shows simulation parameters at 300 K. Between 50 K and 300 K, the mobility varies as [25]

$$\mu = \mu_0 T^{-2.65} \tag{19}$$

And the expression of energy gap is given as [26]

$$E_g(T) = 125 + \sqrt{400 + 0.256 \times T^2} \tag{20}$$

At 300 K, the total effective R_0A product is around 1.3×10^{-4} ohm·m^2. At 240 K, the total effective R_0A product is around 1.6×10^{-4} ohm·m^2. When temperature is higher, the total effective R_0A product becomes smaller. According to Equation (10), **Figure 4** gives the results of the total effective R_0A product on the

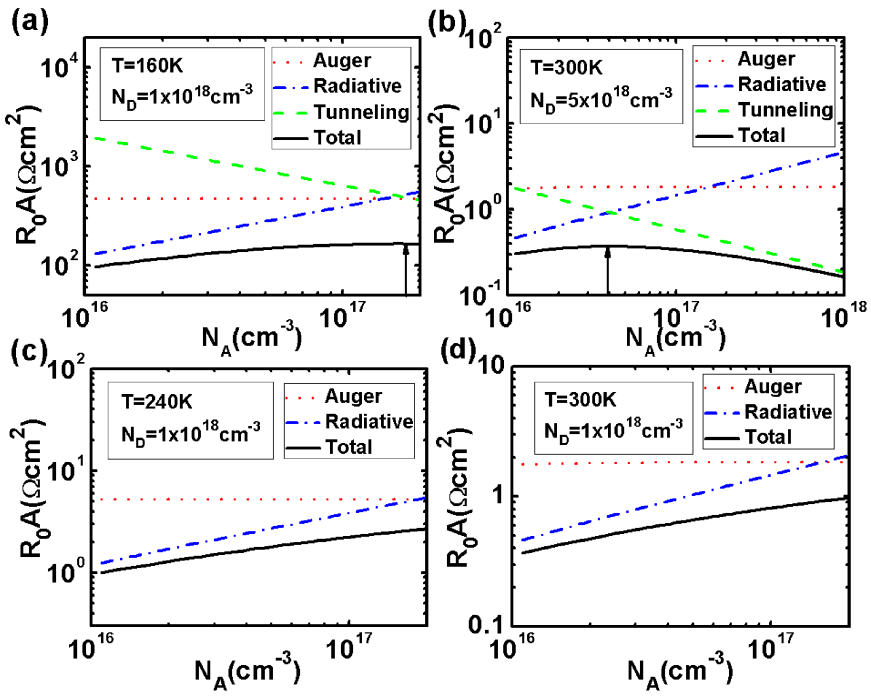

Figure 4. The PbSe R_0A product determined by the diffusion current in the case of Auger recombination and radiative recombination at different high temperature. The black curve is the total effective PbSe R_0A product on the diffusion current in the case of Auger recombination and radiative recombination.

Table 2. The parameters are applied in the simulations for 300 K [27].

Eg(eV)	0.278 eV
P_l(eVcm)	3.9×10^{-8}*
P_t(eVcm)	2.9×10^{-8}*
μ(cm^2/Vs)	200
ε_s	203
ε_∞	22.9

diffusion current in the case of Auger recombination and radiative recombination at a different temperature. At 160 K, tunneling R_0A value is comparable to the Auger and radiative R_0A value.

Figure 4(a) shows the R_0A limitation at 160 K when the n$^+$ doping concentration is $N_D = 1\times10^{18}\,\mathrm{cm}^{-3}$. In this case, $(R_0A)_T$ is comparable with $(R_0A)_{RA}^{-1}$ and $(R_0A)_{Auger}^{-1}$. When the tunneling effect on the total R_0A cannot be ignored, there exists an optimized carrier concentration for the largest R_0A. In this case, the largest R_0A occurs at $N_A = 1.8\times10^{17}\,\mathrm{cm}^{-3}$. When the n side carrier concentration was increased from $1\times10^{18}\,\mathrm{cm}^{-3}$ to $5\times10^{18}\,\mathrm{cm}^{-3}$, tunneling could not be ignored at 300 K, as shown in **Figure 4(b)**. The contribution from tunneling recombination results in a lower total R_0A in **Figure 4(b)**. In **Figure 4(c)** and **Figure 4(d)**, where tunneling can be ignored, it seems that higher PbSe doping concentration (N_A) gives a larger total R_0A. This is because a larger N_A leads to a

smaller minority carrier concentration, which in turn reduces the saturation current. However, for a n^+-p junction n-doping concentration has to be increased, as p-doping concentration increases, which will increase the tunneling effect. In our simulations, the maximum R_0A limit at 240 K (Figure 2(c)) and room temperature (Figure 2(d)) occurs when carrier concentration on the p side is at a maximum, while satisfying the condition for the n^+-p junction where $N_D = 1\times10^{18}\text{cm}^{-3}$ and $N_A = 2\times10^{17}\text{cm}^{-3}$. The recombination mechanisms in n^+ side are not taken into consideration in this paper. Recombination in n^+ side poses a further limitation of n^+ concentration and thus p-doping concentration for optimized D^*. Assuming a wide bandgap N^+-doping layer with negligible Auger and Radiative recombination rate, and negligible tunneling effect, then higher p-type doping concentration could be used to further increase the R_0A.

4. Thermal Noise and Background Photon Shot Noise

As can be seen from Equation (6), the two main mechanisms contributing to the homojunction device are the thermal noise and the background photon shot noise. By using calculated R_0A when $N_D = 1\times10^{18}\text{cm}^{-3}$ and $N_A = 2\times10^{17}\text{cm}^{-3}$, the temperature dependence current noise of these two sources is described in Figure 5.

From Figure 5, we can easily see that at room temperature the dominant source of noise in the device is the Johnson noise. For temperatures around 191 K to 244 K, the contribution of both noise sources is in the same order of magnitude. Below 200 K, photon noise becomes the dominating mechanism, with the background photon noise current five times greater than the Johnson noise. Therefore, if we ignore one noise source when it is five times lower than the other source, the detectivity expressed in (7) can be simplified to high temperature Johnson noise limited D^* and background limited infrared photodetector (BLIP) D^*.

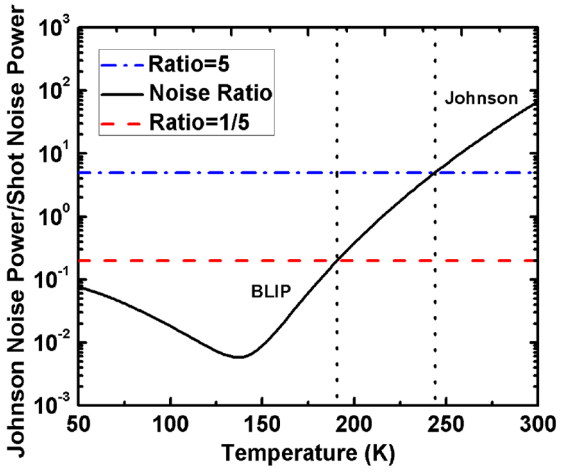

Figure 5. The comparison between the thermal noise and photon background noise on PbSe PV detectors related to temperature.

$$D^* = \frac{q\eta\lambda}{hc}\left[\frac{4kT}{R_o A}\right]^{-1/2} \quad \text{for } T > 244 \text{ K} \tag{21}$$

$$D^* \equiv D^*_{BLIP} = \frac{q\eta\lambda}{hc}\left[2q^2\eta\Phi_b\right]^{-1/2} \quad \text{for } T < 191 \text{ K} \tag{22}$$

5. Theoretical Limitation on the Specific Detectivity D^* at High Temperature

To find the theoretical limit for PbSe photovoltaic detector D^* at 300 K, we apply the R_0A product from the above conditions with Equation (23) because photon shot noise can be negligible at room temperature.

$$D^* = \frac{q\eta\lambda}{hc}\left[\frac{4kT}{R_o A}\right]^{-1/2} \tag{23}$$

At 240 K, to calculate the theoretical limit for PbSe photovoltaic detector D^* following by:

$$D^* = \frac{q\eta\lambda}{hc}\left[\frac{4kT}{R_o A} + 2q^2\eta\Phi_b\right]^{-1/2}, \quad \Phi_b = 1.23\times10^{16} \text{ cm}^{-2}\cdot\text{sec}^{-1} \tag{24}$$

Theoretically, the quantum efficiency should be calculated by the number of electron-hole pairs generated per incident photon. In order to get the D^* limitation, the detector quantum efficiency is simplified to a constant for a different cutoff wavelength. The D^* of the PbSe junction is simulated for a quantum efficiency of 75% and 100%, λ is the wavelength of the incident radiation, q is the charge of the carrier, h is Planck's constant, c is the speed of light, k is Boltzmann's constant, R_0 is the diode incremental resistance at 0 V, A is the detector sensitive area, T is the temperature of the detector in Kelvin. With cutoff wavelength λ = 5 μm at T = 240 K, the photon flux Φ_b equals to 1.23×10^{16} cm^{-2} sec^{-1}. **Figure 6** shows D^* for the PbSe junction as it depends on the absorbing light wavelength at 240 K and 300 K. At 300 K with 100% quantum efficiency, the theoretical limit of D^* for the photovoltaic PbSe n^+-p junction detector is 2.8×10^{10} $\text{HZ}^{1/2}$/W at 4.5 μm. At 240 K, the D^* theoretical limit is 3.7×10^{10} $\text{HZ}^{1/2}$/W at the cut-off wavelength of 5 μm.

Due to reabsorption in the crystal, the effect of radiative recombination may be reduced and carrier radiative life time becomes larger [28]. Photon reabsorption is an effect by which a photon created by the recombination of an electron-hole pair is reabsorbed to produce a new pair and the process is repeated over and over again until a photon can either escape from the sample, or is absorbed by a process which does not create electron-hole pairs, such as free carrier absorption [29]. Considering this, Auger recombination becomes the dominating mechanism at high temperature. The D^* of the PbSe junction in this case is shown in **Figure 7**.

At 300 K, the limitation of D^* now increases from 2.8×10^{10} $\text{HZ}^{1/2}$/W to 3.9×10^{10} $\text{HZ}^{1/2}$/W at 4.5 μm when radiative recombination is ignored.

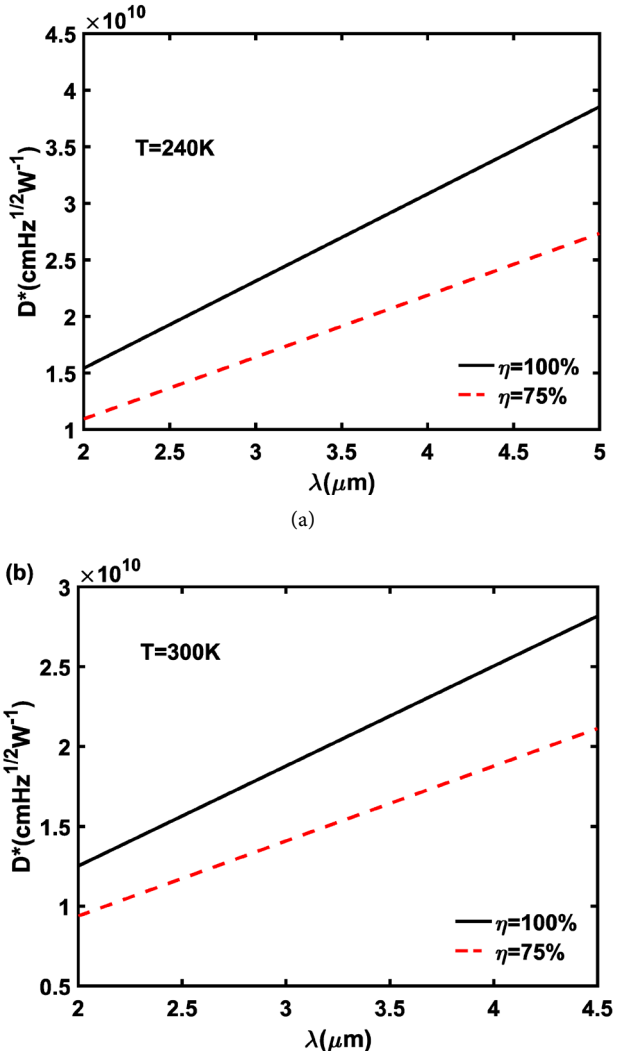

Figure 6. The specific detectivity D^* on the PbSe junction versus the absorbing light wavelength at 240 K and 300 K.

In this n^+-p homojunction junction model, the n^+ PbSe was not considered for its impact on diffusion R_0A product. As discussed in previous sections, high carrier concentration will lead to high Auger and radiative recombination and thus reduced R_0A product. To achieve the calculated D^* in this paper, a heterojunction structure with a wide bandgap N^+ doped layer with much reduced Auger and radiative recombination is needed.

6. Optimization on Carrier Concentration

According to **Figure 4(a)**, when tunneling can be ignored, R_0A value increases with increasing N_A. However, to keep the device n^+-p junction N_D needs to be increased with N_A, which increases the tunneling effect. Therefore, there exists an optimized N_A which provides the maximum R_0A at a given temperature. In the following calculation, N_D/N_A is set to be 5 to satisfy the condition for a n^+-p

junction. N_A is then optimized at 300 K and 240 K, as show in Figure 8. The optimized R_0A for PbSe homojunction at 300 K and 240 K are 2.5×10^{18} cm^{-3} and 1.5×10^{18}, respectively. For optimized carrier concentration the detector reaches BLIP limited D^* at 210 K, 10 degrees higher than the "typical" carrier concentration.

At 240 K, the optimized $N_D = 1.5 \times 10^{18} cm^{-3}$ and $N_A = 3 \times 10^{18} cm^{-3}$ are used to calculate maximum R_0A product in Figure 9(a). By using the maximum R_0A value, the limitation D^* is increased to 5.6×10^{10} $HZ^{1/2}/W$. At 300 K, the optimized $N_D = 2.5 \times 10^{18}$ and $N_A = 5 \times 10^{17} cm^{-3}$ are applied to get the limitation D^* which can be increased to 3×10^{10} $HZ^{1/2}/W$ in Figure 9(b). Therefore, at different temperatures the carrier concentration can be optimized to achieve the highest D^*.

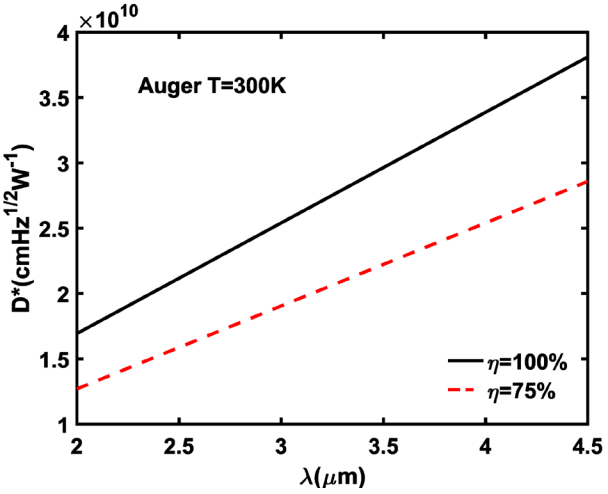

Figure 7. The specific detectivity D^* on the PbSe junction with Auger limitation versus the absorbing light wavelength at 300 K.

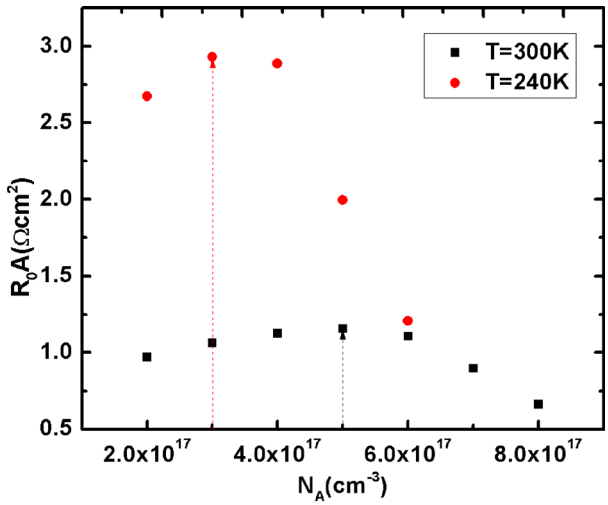

Figure 8. The n side doping concentration dependent PbSe R_0A products at 240 K and 300 K.

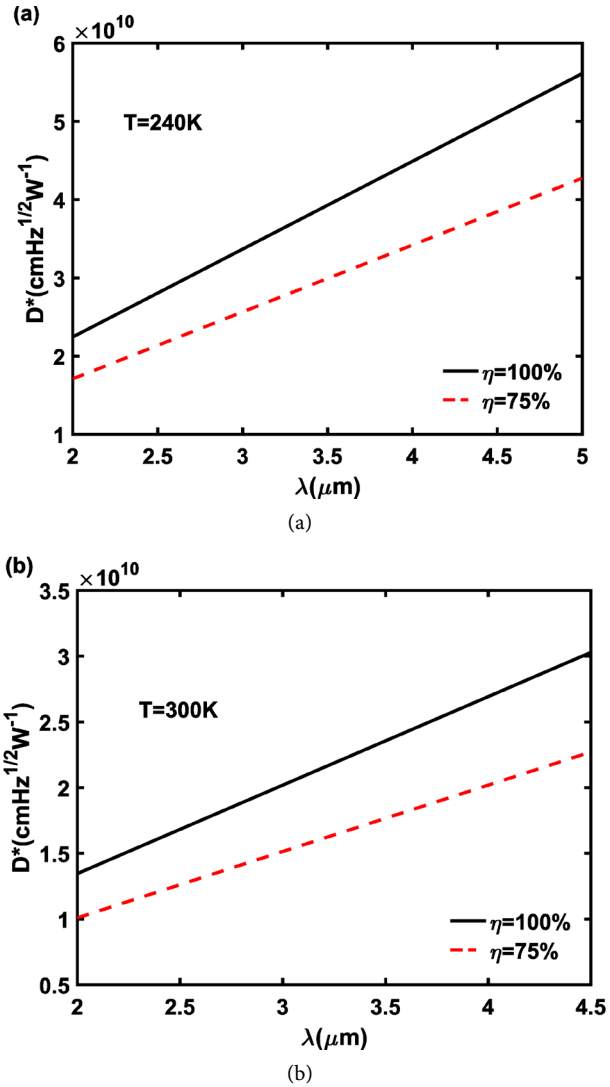

Figure 9. D* versus wavelength at 240 K and 300 K after carrier concentration optimization.

7. Conclusion

Performance limitation of the PbSe homojunction at high temperatures is theoretically studied in this paper. For such PV detectors thermal noise is dominating at temperatures higher than 240 K. BLIP limit could be achieved at temperatures around 210 K. The calculated peak D^* are 3×10^{10} $HZ^{1/2}/W$ and 5.6×10^{10} $HZ^{1/2}/W$ at 300 K and 240 K respectively. Achieving D^* of more than 10^{10} $HZ^{1/2}/W$ in a MWIR detector at uncooled temperatures allows for its use in practical applications of high sensitivity.

Acknowledgements

The authors thank helpful discussions with Dr. Sung-Shik Yoo from Northrop Grumman. This work is partially supported by the DARPA WIRED program through Northrop Grumman, US army research office (ARO) under Grant No.

W911NF-14-1-0312. The views, opinions and/or findings expressed are those of the author and should not be interpreted as representing the official views or policies of the Department of Defense or the U.S. Government.

References

[1] Norton, P.R. (1991) Infrared Image Sensors. *Optical Engineering*, **30**, 1649-1663. https://doi.org/10.1117/12.56001

[2] Rogalski, A. (2001) Infrared Detectors. 2 Edition, Taylor and Francis Group, LLC and. CRC Press, New York.

[3] Tennant, W.E. (2011) Limits of Infrared Imaging. *International Journal of High Speed Electronics and Systems*, **20**, 529-539. https://doi.org/10.1142/S0129156411006829

[4] De Wames, R.E. and Pellegrino, J.G. (2012) Electrical Characteristics of MOVPE grown MWIR N^+p(As)HgCdTe Heterostructure Photodiodes Build on GaAs Substrates. In: Andresen, B.F., Fulop, G.F. and Norton, P.R., Eds., *Infrared Technology and Applications XXXVIII*, Proceeding of SPIE Vol. 8353 83532K-1, Baltimore.

[5] Klann, R., Hofer, T., Buhleier, R., Elsaesser, T. and Tomm, J.W. (1995) Fast Recombination Processes in Lead Chalcogenide Semiconductors Studied via Transient Optical Nonlinearities. *Journal of Applied Physics*, **77**, 277. https://doi.org/10.1063/1.359388

[6] Findlay, P.C., Pidgeon, C.R., Murdin, B.N., van der Meer, A.F.G., Langerak, A.F.G., Ciesla, C.M., Oswald, J., Springholz, G. and Bauer, G. (1998) Auger Recombination Dynamics of Lead Salts under Picosecond Free-Electron-Laser Excitation. *Physical Review B*, **58**, 12908. https://doi.org/10.1103/PhysRevB.58.12908

[7] Ziep, O., Mocker, O., Genzow, D. and Hermann, K.H. (1978) Auger Recombination in PbSnTe-Like Semiconductors. *Physica Status Solidi B*, **90**, 197. https://doi.org/10.1002/pssb.2220900121

[8] Yongdale, E.R., Meyer, J.R., Hoffman, C.A., Bartoli, F.J., Grein, C.H., Young, P.M., Ehrenreich, H., Miles, R.H. and Chow, D.H. (1994) Auger Lifetime Enhancement in InAs-$Ga_{1-x}In_xSb$ Superlattices. *Applied Physics Letters*, **64**, 3160. https://doi.org/10.1063/1.111325

[9] Meyer, J.R., Felix, C.L., Bewley, W.W., Vurgaftman, I., Aifer, E.H., Olafsen, L.J., Lindle, J.R., Hoffman, C.A., Yang, M.-J., Bennett, B.R., Shanabrook, B.V., Lee, H., Lin, C.-H., Pei, S.S. and Miles, R.H. (1998) Auger Coefficients in Type-II InAs/$Ga_{1-x}In_xSb$ Quantum Wells. *Applied Physics Letters*, **73**, 2857. https://doi.org/10.1063/1.122609

[10] Young, P.M., Grein, C.H., Ehrenreich, H. and Miles, R.H. (1993) Temperature Limits on Infrared Detectivities of InAs/$In_xGa_{1-x}Sb$ Superlattices and Bulk $Hg_xCd_{1-x}Te$. *Journal of Applied Physics*, **74**, 4774. https://doi.org/10.1063/1.354348

[11] Ciesla, C.M., Murdin, B.N., Phillips, T.J., White, A.M., Beattie, A.R., Langerak, G.M., Elliott, C.T., Pidgeon, C.R. and Sivananthan, S. (1997) Auger Recombinatin Dynamics of $Hg_{0.795}Cd_{0.205}Te$ in the High Excitation Regime. *Applied Physics Letters*, **71**, 3160. https://doi.org/10.1063/1.119588

[12] Beattie, A.R. and White, A.M. (1996) An Analytic Approximation with a Wide Range of Applicabilty for Electron Initiated Auger Transitions in Narrow-Gap Semiconductors. *Journal of Applied Physics*, **79**, 802. https://doi.org/10.1063/1.360828

[13] Qiu, J., Weng, B., Yuan, Z. and Shi, Z. (2013) Study of Sensitization Process on

Mid-Infrared Uncooled PbSe Photoconductive Detectors Leads to High Detectivity. *Journal of Applied Physics*, **113**, 103102. https://doi.org/10.1063/1.4794492

[14] Weng, B., Qiu, J., Yuan, Z., Larson, P., Strout, G. and Shi, Z. (2014) CdS/PbSe Heterojunction for High Temperature Mid-Infrared Photovoltaic Detector Applications. *Applied Physics Letters*, **104**, 121111. https://doi.org/10.1063/1.4869752

[15] Zhao, L., Qiu, J., Weng, B., Chang, C., Yuan, Z. and Shi, Z. (2014) Understanding Sensitization Behavior of Lead Selenide Photoconductive Detectors by Charge Separation Model. *Journal of Applied Physics*, **115**, Article ID: 084502. https://doi.org/10.1063/1.4867038

[16] Green, K., Yoo, S.-S. and Kauffman, C. (2014) Lead Salt TE-Cooled Imaging Sensor Development. *Proceedings of the SPIE*, **9070**, 90701G.

[17] Driggers, R. (2014) What's New in Infrared Systems? http://spie.org/x106781.xml https://doi.org/10.1117/2.4201404.12

[18] Clark Jones, R. (1953) Performance of Detectors for Visible and Infrared Radiation. *Advances in Electronics and Electron Physics*, **5**, 1-96.

[19] Rogalski, A. (2011) Infrared Detectors. 2nd Edition, Taylor and Francis Group and CRC Press, Boca Raton, 34-35.

[20] Buckingham, M.J. and Faulkner, E.A. (1974) The Theory of Inherent Noise in p-n Junction Diodes and Bipolar Transistors. *Radio and Electronic Engineer*, **44**, 125-140. https://doi.org/10.1049/ree.1974.0036

[21] Johnson, M.R., Chapman, R.A. and Wrobel, J.S. (1975) Detectivity Limits for Diffused Junction PbSnTe Detectors. *Infrared Physics*, **15**, 317-329. https://doi.org/10.1016/0020-0891(75)90050-0

[22] Rogalski, A., Adamiec, K. and Rutkowski, J. (2000) Narrow Gap Semiconductor Photodiodes.

[23] Preier, H. (1979) Recent Advances in Lead-Chalcogenide Diode Lasers. *Applied Physics*, **20**, 189-206. https://doi.org/10.1007/BF00886018

[24] Rogalski, A. (2011) Infrared Detectors. CRC Press, Boca Raton.

[25] Schlichting, U. and Gobrecht, K.H. (1973) The Mobility of Free Carriers in PbSe Crystals. *Journal of Physics and Chemistry of Solids*, **34**, 753-758. https://doi.org/10.1016/S0022-3697(73)80183-0

[26] Lu, X. and Shi, Z. (2005) Theoretical Investigations of [110] IV-VI Lead Salt Edge-Emitting Lasers. *IEEE Journal of Quantum Electronics*, **41**, 308-315. https://doi.org/10.1109/JQE.2004.841607

[27] Rogalski, A., Ciupa, R. and Zogg, H. (1995) Solid State Crystals: Materials Science and Applications. International Society for Optics and Photonics, Bellingham.

[28] Parrot, J.E. (1993) Radiative Recombination and Photon Recycling in Photovoltaic Solar Cells. *Solar Energy Materials and Solar Cells*, **30**, 221-231. https://doi.org/10.1016/0927-0248(93)90142-P

[29] Weiser, K., Ribak, E., Klein, A. and Ainhorn, M. (1981) Recombination of Photocarriers in Lead-Tin Telluride. *Infrared Physics*, **21**, 149-154. https://doi.org/10.1016/0020-0891(81)90022-1